



CO₂ adsorption by KOH-activated hydrochar derived from banana peel waste

Chirag Goel¹ · Sooraj Mohan² · P. Dinesha¹ · Marc A. Rosen³

Received: 19 May 2023 / Accepted: 31 January 2024 / Published online: 27 February 2024
© The Author(s) 2024

Abstract

Hydrothermal carbonization is one of the effective methods of converting wet lignocellulosic biomass into carbon-rich hydrochar. Due to its characteristic application on CO₂ capture and storage, many researchers have studied the CO₂ uptake on activated hydrochar. The present work studies the CO₂ uptake from banana-peel-derived activated hydrochar which is not presented in the literature. Hydrochar is obtained at three different temperatures (180, 200, and 220 °C) and activated using KOH. Characterization studies including SEM, XRD and FTIR were performed to examine the structure and chemistry of the derived activated hydrochar. The hydrochar sample (BP-180) when activated with a KOH/hydrochar ratio of 3 and an activation temperature of 700 °C has a well-developed microstructure with a surface area and pore volume of 243.4 m²/g and 0.0931 cm³/g, respectively. Samples obtained at higher process temperatures (BP-200 and BP-220) showed much lower porosity. Similarly, the maximum CO₂ adsorption is recorded for BP-180 (3.8 mmol/g), followed by BP-200 and BP-220 with maximum adsorption capacities of 3.71 and 3.18 mmol/g, respectively, at 1 bar and 25 °C.

Keywords Activated carbon · CO₂ adsorption · Banana peel waste · Hydrochar · Climate change

Abbreviations

BP	Banana peel
BP-180	Banana peel hydrochar at 180 °C HTC temperature
BP-200	Banana peel hydrochar at 200 °C HTC temperature
BP-220	Banana peel hydrochar at 220 °C HTC temperature
EDX	Energy-dispersive X-ray spectroscopy
FTIR	Fourier transform infrared spectroscopy
HTC	Hydrothermal carbonization
KOH	Potassium hydroxide
Θ	X-ray diffraction angle (degree)

ppm	Parts per million
S _{BET}	Brunauer–Emmett–Teller surface area (m ² /g)
SEM	Scanning electron microscope
V _t	Total pore volume (cm ³ /g)
XRD	X-ray diffraction

Introduction

CO₂ has been the most significant contributor (about 65%) to global greenhouse gas emissions. CO₂, CH₄, and N₂O are greenhouse gases that play significant roles in climate change. The rapid annual growth rate of atmospheric CO₂ concentration of about 3.4 ppm per year has increased the concentration to 417 ppm by November 2022 (Global Monitoring Laboratory 2022). Rapid industrialization, deforestation and overpopulation are significant reasons for the rise in atmospheric CO₂ levels. In 2019, greenhouse gas emissions reached an all-time high of 52.4 gigatons of CO₂ equivalent, mainly due to a 0.9% annual increase in fossil CO₂ emissions (Olivier and Peters 2020). Though there was a slight decrease in emissions in the European Union, the USA and Japan, increased emissions were reported in India, Russia and China. Global warming and climate change have been the main reasons for the rise in temperature, low rainfall

✉ P. Dinesha
dinesha.p@manipal.edu

¹ Department of Mechanical and Industrial Engineering, Manipal Institute of Technology, Manipal Academy of Higher Education, Manipal 576104, India

² Department of Mechanical Engineering, National Institute of Technology Goa, Salcette Taluka, Cuncolim, Goa 403703, India

³ Faculty of Engineering and Applied Science, University of Ontario Institute of Technology, 2000 Simcoe Street North, Oshawa, ON L1G 0C5, Canada

and seasonal fluctuations in food production which have further reduced global agricultural output (Sekoai and Yoro 2016). A limit of global warming below 2 °C has been recommended by the 2015 Paris agreement, compared to pre-industrial levels. At least one gigaton of CO₂ must be stored annually until 2030 to achieve the target set in this agreement (van Soest et al. 2017).

Carbon capture and storage (or carbon capture and sequestration) is one of the ways to mitigate CO₂ emissions. With such technology, CO₂ is captured and stored (e.g., deep underground in suitable geological formations (Hong 2022)). Carbon capture and storage methods can be categorized into three primary options: post-conversion, pre-conversion, and oxy-fuel combustion (Cuéllar-Franca and Azapagic, 2015). Post-conversion specifically involves the removal or capture of CO₂ after the combustion process has taken place. While it offers the advantage of easy integration into existing plants, it does come with a significant energy penalty (Leung et al. 2014). Some of the technologies utilized for post-conversion capture include liquid-phase chemisorption technology, adsorption, and calcium looping technology. Adsorption technology is particularly valuable due to its versatility for retrofitting and its capacity to perform effectively under a wide range of pressure and temperature conditions (Bui et al. 2018). Solid CO₂ adsorbents offer several advantages over liquid adsorbents, such as suitability for a broader temperature range, up to 700 °C (Choi et al. 2009), reduced waste generation, and less harmful disposal. Solid CO₂ adsorbents can be further categorized into three groups based on their temperature range. Low-temperature adsorbents (below 200 °C) include carbon-based adsorbents (Deepak et al. 2023), zeolite-based adsorbents (Chue et al. 1995), metal–organic framework-based adsorbents, various alkali-metal carbonate-based adsorbents, and amine-based solid adsorbents. Intermediate-temperature adsorbents (200–400 °C) consist of hydrotalcite-like compound solid adsorbents. High-temperature adsorbents (above 400 °C) encompass calcium-based adsorbents and alkali ceramic-based adsorbents (Wang et al. 2011). Adsorption has gained attention as one of the potential methods for CO₂ removal from flue gases due to its low energy requirements, low capital investment, and high CO₂ capture capacity. Nonetheless, there are still requirements for this technology, e.g., to produce adsorbents with better working capacities, tolerances to impurities and selectivity towards gases (Goel et al. 2021).

Carbon-based adsorbents like activated carbon, hydrochar and biochar are promising adsorbents that can be produced from various raw materials (precursors). They have several advantages over other adsorbents because of their large surface areas, ability for pore structure modification, and ease of renewal, which makes them highly suitable for CO₂ sequestration. Mass production of carbon-based materials is straightforward because of their availability, low cost, and

ease of manufacturing. Carbon-based material is hydrophobic, which increases its usability in humid climates. Hydrochar does not require chemical or physical activation and has low preparation costs and environmental impact. Therefore, biochar and hydrochar have gained popularity as adsorbents for pollutants over other carbon-based adsorbents. Biochar and hydrochar are produced mainly by pyrolysis and hydrothermal carbonization (HTC).

Various biomasses, like corn stover, loblolly pine, tobacco stalk, rice husk, eucalyptus bark, and sweet potato waste, have been discussed as potential precursors for the development of hydrochar and biochar (Goel et al. 2021). The selection of biomass is primarily driven by its yield, CO₂ adsorption capacity, and raw material availability. Biomass for the production of hydrochar and biochar is carbon-based and can be derived from both animal and plant waste. Char synthesis aims to maximize the solid carbon content (Khan et al. 2021). Biomass-derived from plants mainly contains cellulose, hemicellulose, and lignin. An increase in lignin content contributes to char production, whereas volatile material production is primarily stems from cellulose and hemicellulose (Liu et al. 2014). Therefore, for char production, high lignin-content biomasses are more suitable. Minerals and content present in biomass act like a catalyst, affecting the properties and product yield of the outputs of biomass conversion processes like HTC and pyrolysis. The moisture content of the biomass determines the conversion process. Wet biomasses have more than 30% moisture, and dry biomass has less than 30% (Kambo and Dutta 2015). While pyrolysis is used to produce biochar from dry biomass, HTC can be employed to process wet biomass and convert it to hydrochar. Another classification is ‘purpose grown’ and ‘waste biomass’ depending on the source from which it was obtained (Brosse et al. 2012). Purpose-grown biomass has a low moisture (<5%) and is specially grown. This eliminates the need for pre-drying. Waste biomass has no economic value and is suitable for producing char as it is cheap and readily available (Perlack 2003). CO₂ uptake on KOH-activated hydrochar produced by plant waste like water chestnut shells (Li et al. 2020) was reported as 3.61 mmol/g at 25 °C and 600 °C activations. Water caltrop shell (Zhao et al. 2021) and camphor leaves (Xu et al. 2018) hydrochar showed uptakes of 3.71 mmol/g and 3.74 mmol/g, respectively, under the same conditions. A similar CO₂ uptake was noted by (Parshetti et al. 2015) for empty fruit bunch hydrochar when activated with KOH and an activation temperature of 800 °C. Argan shell (Boujibar et al. 2018) hydrochar was shown to have a very high CO₂ uptake of 5.63 mmol/g at 850 °C activation temperature. Rehman et al. studied the CO₂ adsorption on hydrochar derived from orange peel waste where potassium oxalate was used as an activating agent (Rehman et al. 2022). The nitrogen doped hydrochar sample activated at 900 °C exhibited high surface area (2130

m^2/g) and micropore volume ($1.12 \text{ cm}^3/\text{g}$) resulting in high CO_2 uptake at 0°C and 1 bar ($6.6 \text{ mmol}/\text{g}$). Zubbri et al. conducted CO_2 uptake studies on KOH-activated hydrochar obtained from rambutan peel (Zubbri et al. 2021). By activating at 850°C along with an additional water-soaking pretreatment, the CO_2 adsorption of $122 \text{ mg}/\text{g}$ was obtained at 30°C . Deepak et al. studied the CO_2 adsorption performance on orange-peel derived KOH-activated hydrochar (Deepak et al. 2023). The maximum CO_2 uptake of $3.045 \text{ mmol}/\text{g}$ at 25°C was obtained by the hydrochar synthesized at 220°C . A KOH to char ratio of 3 was used, and the hydrochar was activated at a temperature of 700°C .

The information described indicates that no studies have been reported on carbon capture using hydrochar derived from banana peel (BP). According to agricultural production and trade, bananas are a leading crop worldwide. The rapid increase in production and export volume has resulted from rapid population growth in producing countries and expanding global consumption. Bananas have become the world's second-largest fruit crop because of their high consumption and cultivation. According to Mordor Intelligence, global production stood at around 116 million metric tonnes in 2019 and is projected to register a compounded annual growth rate of 4.5% during the forecast period of 2022–2027 (Mordor Intelligence 2022). Asia, Latin America, and Africa are the predominant cultivators of bananas. Between 2010 and 2017, the largest production of bananas came from India (29 million tonnes), followed by China, with 11 million tonnes. Both countries primarily serve their domestic markets. The Philippines with 7.5 million tonnes, and Ecuador, and Brazil, with an annual average of 7 million tonnes each, are other nations with high banana production (Dadrasnia et al. 2020). Production of bananas increased in India to 30.5 million tonnes in 2019 from 2.9 million tonnes in 1970 and is still growing at an average annual rate of over 5%. Such high banana production also means increased availability of BP as waste biomass. Discarded biomass causes wastage of resources and environmental pollution; the transformation of BP into valuable matter can contribute towards sustainability (Yabalak and Elneccar 2022). Raw and treated hydrochar from BP via carbonization at 513 K for 1 h exhibit Brunauer–Emmett–Teller surface areas (S_{BET}) of $7.22 \text{ m}^2/\text{g}$ and $2.86 \text{ m}^2/\text{g}$, respectively, and have corresponding pore diameters of 5.4 nm and 6.07 nm. Applications of BP hydrochar were studied by (Yusuf et al. 2020) where HTC was performed at by varying the temperature from 150 to 300°C for residence times of 1 and 2 h. The surface area of the original feed stalk was increased from $1.1 \text{ m}^2/\text{g}$ to $1.6 \text{ m}^2/\text{g}$ for carbonization at 200°C , and reached an area of $9.2 \text{ m}^2/\text{g}$ at 300°C . About 30–40% of the total fruit weight consists of BP, of which cellulose is approximately 60–65%, while 6–8% is hemicellulose, and 5–10% is lignin (Liew et al. 2018; Pokharel et al. 2018). BP has been used

as fertilizers and even for skin care (Lee et al. 2010; Hussein et al. 2019). An analysis of BP shows that it contains 35.65% carbon, 6.19% hydrogen, 1.94% nitrogen and 45.94% oxygen (Kabenge et al. 2018).

Various methods were employed to fully characterize hydrochar samples derived from BP waste. These methods included BET surface area analysis, thermo-gravimetric analysis (TGA), X-ray diffraction (XRD), scanning electron microscopy-energy-dispersive X-ray spectroscopy (SEM–EDX), and Fourier-Transform infrared spectroscopy (FT-IR). The investigation revealed distinct morphological and microstructural features of the hydrochar sample. Very few studies have reported on the synthesis of BP waste hydrochar, and literature review indicates that no prior studies have used activated BP hydrochar as an adsorbent for CO_2 , even though it is a low-cost precursor. Hence, the objective of the present work is to address this gap by ascertaining the behaviour of CO_2 adsorption on hydrochar synthesized from BP at different temperatures.

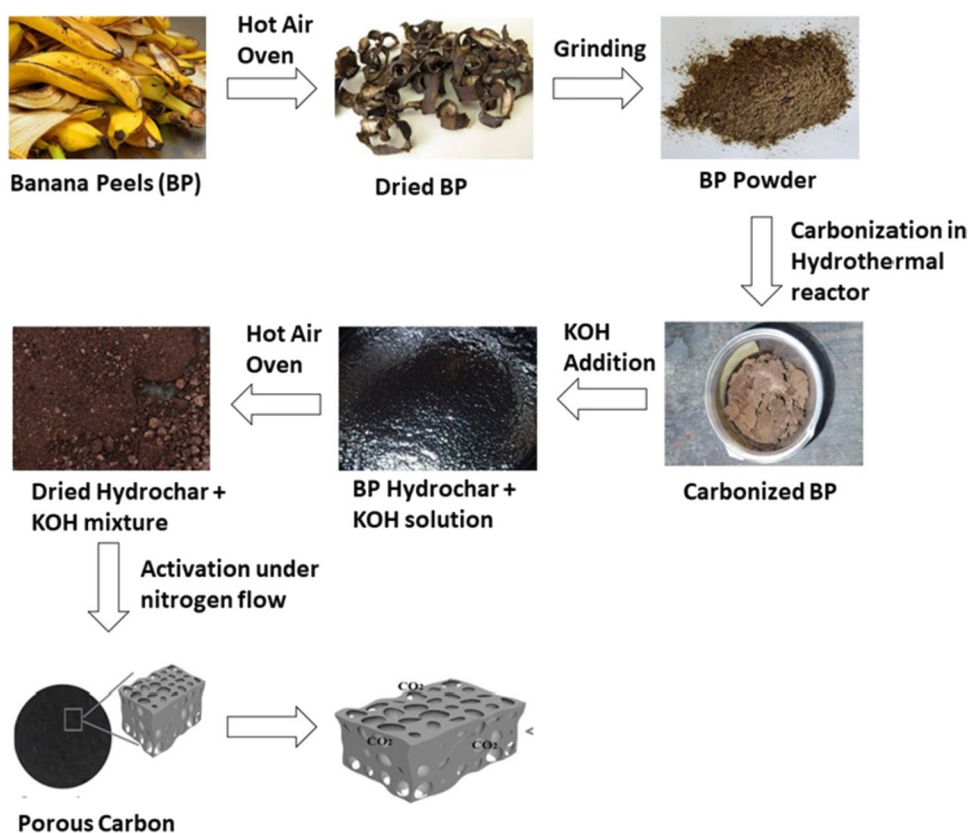
In this study, hydrochar was successfully produced from BP waste via hydrothermal carbonization (HTC) at varying temperatures: 180°C , 200°C , and 220°C , designated as BP-180, BP-200, and BP-220, respectively. The resulting hydrochar was further activated using KOH to enhance its carbon capture properties. The CO_2 adsorption capacities of the prepared sorbents were measured at 25°C and pressures ranging from 0 to 1 bar. The findings demonstrated that BP-180 exhibited superior performance compared to BP-200 and BP-220 in terms of CO_2 uptake. The authors performed a literature review on the char:KOH ratio and concluded that a ratio of 1:3 is optimal for activation. Excess KOH ensured complete activation of the hydrochar. A high KOH ratio also increases the surface development including porosity and surface area which is required for high CO_2 uptake (Singh et al. 2019).

Material and methods

Synthesis of materials

A fixed variety of bananas (Robusta) was collected locally, and the banana were peeled. Further drying of BP at 80°C to 90°C in an oven was carried out until a constant weight was obtained. The masses of banana peels after drying were measured, and the percentage of biomass recovered after drying was 9.90%. After drying of the banana peels, they were ground to a fine powder. The obtained fine powder was then sieved through a wire mesh of size 20 μm to obtain a uniform particle size. This powder obtained was then used for hydrochar production using the hydrothermal carbonization process. The synthesis procedure for activated hydrochar is shown in Fig. 1. The reactor was equipped

Fig. 1 Processing steps in the conversion of biomass to hydrochar



with sensors to measure temperature and pressure during the process of HTC. The temperature inside the reactor was controlled by an electric band heater by adjusting the input electric voltage. 4 g of dried and fine ground BP was dispersed into 60 mL of water and placed in a 100 mL Teflon-lined reactor for the HTC process. The ratio of biomass to water was maintained at 1:15 by mass. Hydrothermal carbonization was then performed at three temperatures, 180 °C, 200 °C and 220 °C, for 3 h after the required temperature was reached and the corresponding samples were designated BP-180, BP200, and BP-220. The temperature was maintained by adjusting the saturated pressure to the corresponding temperature value. The reactor was allowed to cool to room temperature before char collection. The char was collected by filtration using Whatman Grade 1 filter paper (particle retention of 11 µm), and dried at 80 °C until a constant weight was obtained. For chemical activation using KOH, the samples were then mixed with an aqueous 6 molar KOH solution in the desired weight ratio (1:3) with a magnetic stirrer for 6 h before drying them in a hot air oven at 90 °C. The KOH aqueous solution was obtained by dissolving 15 g of 99.9% pure KOH pellets with approximately 45 g of water. The hydrochar samples obtained from KOH activation were dried in a hot-air oven at 80 °C until a constant weight was obtained. The dried samples were neutralized with hydrochloric acid (HCl) and deionized water to remove

impurities. Finally, the obtained microporous carbons were dried in an oven at 80 °C. The KOH-treated dried carbon samples were activated in an inert (nitrogen) atmosphere at 700 °C for 2 h. The three samples of the hydrochar obtained at temperatures 180 °C, 200 °C, and 220 °C are named BP-180, BP-200, and BP-220, respectively.

Material characterization

Physical and chemical properties of the synthesised hydrochar were measured before CO₂ adsorption studies were conducted. Specific surface area and pore volume were measured with Brunauer–Emmett–Teller (BET) analysis using a Micromeritics Quantachrome Analyzer. The carbon structures were examined by powder X-ray diffraction (XRD) in a JEOL X-ray diffractometer (DX-GE-2P, Japan make). The incident radiation was Cu K α ($\lambda = 1.5418 \text{ \AA}$) over a range of 2 θ angles from 5 to 90°. The scanning speed was 0.5°/min, and the operating current and voltage were 20 mA and 30 kV, respectively. The morphology and elemental composition were observed using scanning electron microscopy (SEM) (Carl Zeiss, Germany make) and energy-dispersive spectroscopy (EDS) (Link ISIS-300 Micro-analytical System, Oxford instruments, UK). Hydrochar samples were gold sputtered using a JFC 1600 auto fine coater (JEOL, Japan make) before the SEM analysis.

For elemental analysis of samples using EDS, X-ray were emitted on the samples and response was measured. The spectrum obtained was mapped to the pattern of individual elements to determine the chemical composition of sample. The presence of the function group was measured by FTIR spectroscopy (Shimadzu IRSpirit, Japan) in the wave number range of 4000–400 cm^{-1} with resolution of 1 cm^{-1} and average of 32 scans. CO_2 uptake was assessed using a Micromeritics 3Flex Physisorption instrument.

CO_2 adsorption

CO_2 adsorption measurement was performed using thermogravimetry analysis (TGA). TGA measures the change in the sample's mass as a function of temperature over time. TGA analysis was carried out using a 3FLEx 3500 analyzer (Micromeritics Instruments). For each test, approximately 25–30 mg of hydrochar sample was heated slowly to eliminate any pre-adsorbed CO_2 and water. After 60 min of conditioning, the sample was cooled to 25 °C and subjected to a dry mixture of CO_2 and N_2 until sufficient equilibrium was obtained. The CO_2 adsorption was assessed by an increase in mass when the environment was switched from N_2 to CO_2 at 25 °C. The pressure was increased from absolute vacuum to 760 mm Hg, and the CO_2 adsorption was measured at a prefixed equilibration time of 10 s. The amount of CO_2 adsorbed was measured in terms of the change in the mass of the activated hydrochar.

Optimal conditions for production for hydrochar

Temperature

The reaction temperature has a strong influence on the end-product yield. It also affects properties like surface area and pH of char compared to other parameters. Break down and rearrangement of hydrocarbon molecules occur at high temperatures, which results in the release of liquid and gaseous products and a decrease in solid char yield. An increase in HTC reaction temperature will result in a reduction of solid hydrochar yield. Compared to other parameters like residence time and heating rate, reaction temperature

significantly affects the characteristics and yield in the HTC process. HTC reaction temperatures were selected between 180 and 220 °C for analysis as it is optimal for CO_2 adsorption and gives a good yield (Goel et al. 2021; Khan et al. 2021).

Reaction time

The period for which the biomass decomposes in the reactor at a set temperature is known as residence time. A longer reaction time can positively affect the energy density and result in the formation of the secondary hydrochar, which shows a polyaromatic structure. At the same time, higher hydrochar content is obtained when the temperature is lower. A shorter residence time results in higher hydrochar yield in the HTC process. Work has been done for a residence time from 0.5 to 24 h (Dong et al. 2019). For CO_2 adsorption, the optimal residence time of 3 h has been selected.

Results and discussion

Yield and physicochemical properties

The ultimate and proximate analyses of the BP hydrochar sample are shown in Table 1; the table also compares the values with BP biomass. The results show that the carbon content of all samples decreased with increasing temperature while the oxygen content increased. The experiment was repeated three times, and since the values were close, average values were calculated and noted. The hydrochar yield decreased gradually from 45.3% (BP-180) to 42.6% (BP-200), as temperature increased from 180 to 200 °C, respectively. A further increase in temperature to 220 °C decreased the yield to 39.2%. The breakdown of hemicellulose, cellulose, and part of the lignin resulted in a reduction in yield. Yield loss is mainly in the form of volatile material, and various other reactions, like hydrolysis and decomposition, that occur simultaneously. This process depends on temperature as an increase in temperature generally leads to more decomposition of hydrochar into volatile products (Sharma and Dubey 2020).

Table 1 Yield and physicochemical properties of BP hydrochar obtained in this work

Property	C (%)	O (%)	N (%)	H (%)	Yield (%)	O/C ratio	HTC time (h)	References
Raw BP	41.3	53.8	–	4.9	0	0.98	0	Yusuf et al. (2020)
BP-180	80.63	18.07	0	0	45.3	0.22	3	
BP-200	76.93	19.61	0	0	42.6	0.25	3	
BP-220	75.42	20.39	0	0	39.2	0.27	3	
HCT-200	60.7	32.8	0.6	5.9	–	0.41	2	Yusuf et al. (2020)
HCT-250	67.8	25.5	0.9	5.8	–	0.28	2	Yusuf et al. (2020)

Table 1 compares the composition of hydrochar obtained in this and previous studies. It is observed that the hydrothermal carbonization process of BP waste leads to an increase in carbon content from 41.3% (Yusuf et al. 2020) to 80.6% at a 180 °C reaction temperature. A reduction in the carbon composition by 4.5% and 5.2% was observed when the temperature increased to 200 and 220 °C, respectively. An earlier study under the same conditions showed 60.7% and 67.8% of elemental carbon in hydrochar was obtained at 200 °C and 250 °C, respectively (Yusuf et al. 2020). The difference is likely due to the shorter residence time, since complete decomposition and subsequent release of volatile matter of biomass took place.

The oxygen content of the BP and hydrochars obtained in this study were 53.8% and 20.4–18.1%, respectively. The dehydration and decarboxylation reactions are attributed to the decline in the elemental oxygen composition in the hydrochar. Compared to previous studies, the elemental oxygen in BP hydrochar in this study was lower than the values (25.2–32.8%) reported elsewhere (Yusuf et al. 2020).

Hydrogen traces were not discovered in the elemental analysis, which suggests a loss of hydroxy functional groups during activation with KOH (Zubbri et al. 2021). The nitrogen content in BP is less than 2%. Therefore, it is understood that nitrogen is degraded under the HTC process, and traces are below the limit of detection.

FTIR analysis of functional group in hydrochar

The FTIR spectra of all the hydrochar samples for various HTC process temperatures are shown in Fig. 2. Differences can be observed between samples carbonized at different temperatures, confirming the occurrence of chemical transformation during HTC. Peaks between wavenumbers 1720.5 and 1683.9 cm^{-1} were associated with the C=O stretch in carbonyl compounds like ketone, aldehydes, esters, or carboxyl groups caused by the opening of the glycosidic rings of the cellulose and lignin. Energy-dispersive X-ray spectroscopy (EDX) analysis did not detect a trace of hydrogen in any of the hydrochar samples, which indicates the presence of the ketone and ester functional groups. Note also that the absorbance peak decreases significantly with temperature rise, suggesting a loss of oxygen-containing functional groups. Peaks between wavenumbers 1585.5–1521.8 cm^{-1} were ascribed to C=C stretching in aromatic groups and the peaks between wavenumbers 1234.4–1217.1 cm^{-1} are concerned with the C–O stretching in alkyl-substituted ether, cyclic ethers or aromatic ethers, and the aryl-O group. The intensity of peaks decreases with increasing temperature, suggesting lignin decomposition. For the BP-180 and BP-200 samples, strong peaks related to C=C stretching between wavenumbers 1585.5–1521.8 cm^{-1} are found, whereas this peak has reduced intensity for BP-220.

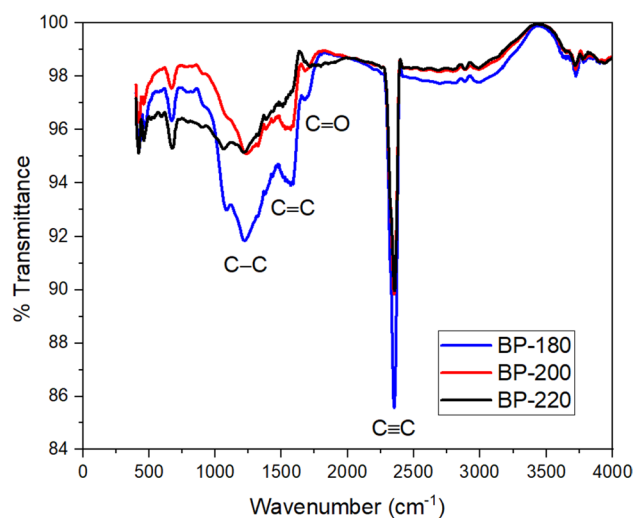


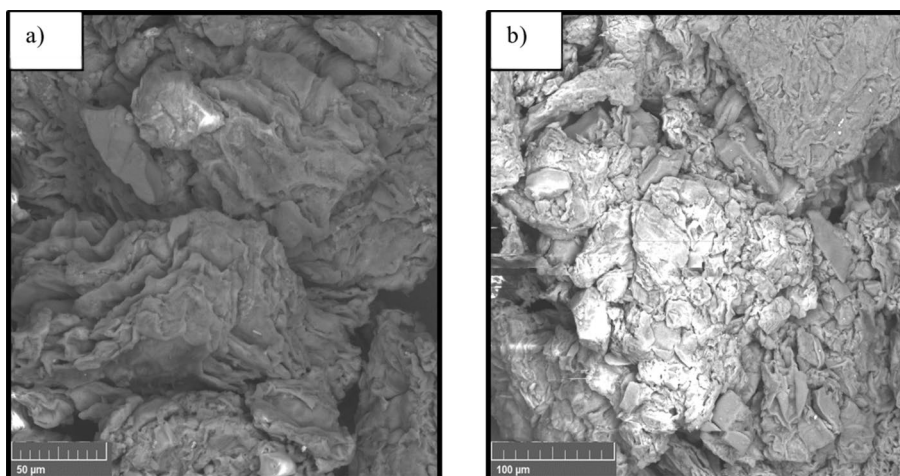
Fig. 2 FTIR analysis of functional group in activated BP hydrochar samples

Therefore, for the optimal formation of aromatic groups, the temperature ranges from 80 to 200 °C (Yusuf et al. 2020). The absence of –OH signals is related to breaking hydrogens bonds, and the development of condensed aromatic structure can be ascertained due to extensive losses of carbonyl, hydroxyl, and C–H groups. C≡C is represented by a peak around wavenumber 2353.2 cm^{-1} and has the sharpest peak in the whole spectra, which means that the char obtains has high carbon content.

SEM analysis for surface characteristics

SEM analysis of BP waste and hydrochar samples reveals important information about the structural changes during hydrothermal carbonization. A rise in temperature during the HTC process leads to degradation, depolymerization reaction, and lignin loss of the biomass. This reaction leads to a small variation in the structural characteristics of the biomass, which can be seen in the magnified SEM images. On close examination of BP waste SEM images, the microscopic surface structure is observed to be dense, impenetrable, and rigid, as shown in Fig. 3. After HTC, the surface structures of all samples exhibit varying porosity, with the sample for BP-180 found to be the most porous. The EDX analysis shows that the hydrochar surface mainly contains carbon, oxygen, and trace amounts of inorganic elements such as Ca, Mg, Si, etc. At higher temperatures, the cellulose and lignin structure in BP may be destroyed, causing the elimination of various functional groups like the hydroxyl, ketone, and aldehyde present in the carbohydrate constituent of BP. This may contribute to the low yield and porosity of BP-200 and BP-220.

Fig. 3 SEM images of BP powder: **a** Scale – 50 μm , **b** Scale – 100 μm



Under HTC conditions, the cellulose and hemicellulose break down, making the hydrochar surface porous. SEM images at a several magnifications of samples subject to HTC are presented and compared in Figs. 4, 5 and 6. The SEM images in this study exhibit an increase in porosity and formation of micropores due to the HTC process and KOH activation. S_{BET} measurement of the sample treated at 180 °C is 243.4 m^2/g ; as the temperature increases to 200 °C, the surface area is measured as 154.6 m^2/g , and on raising the HTC process temperature to 220 °C, the surface area reaches 71.72 m^2/g .

CO₂ sorption analysis

The CO₂ uptake for all hydrochar samples is measured between 0–1 bar pressure and 25 °C. Table 2 summarises the maximum uptakes for all the samples at 1 bar and compares these data with the literature. CO₂ adsorption isotherms for all the samples are shown in Fig. 7. It is observed that the rate of increase in CO₂ adsorption capacity is greater within the low-pressure range (0–0.5 bar) compared to the high-pressure range (0.5–1 bar). The CO₂ uptakes at 25 °C for BP-180 are the highest at 1 bar due to higher surface area and pore volume (243.4 m^2/g and 0.093 cm^3/g , respectively). The CO₂ uptake at 0.15 bar, which is the CO₂ partial pressure in the flue gas, can be as high as 1.4 mmol/g.

Fig. 4 SEM images for activated BP hydrochar (Mag: 35k X): **a** BP-180, **b** BP-200, and **c** BP-220

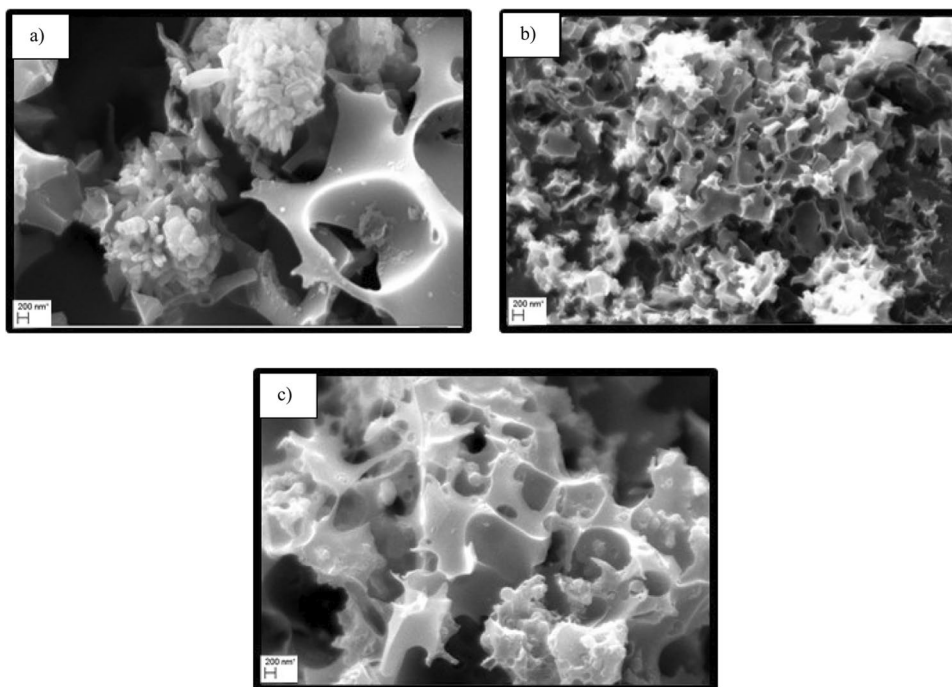


Fig. 5 SEM images for activated BP hydrochar (Mag: 20k X): **a** BP-180, **b** BP-200, and **c** BP-220

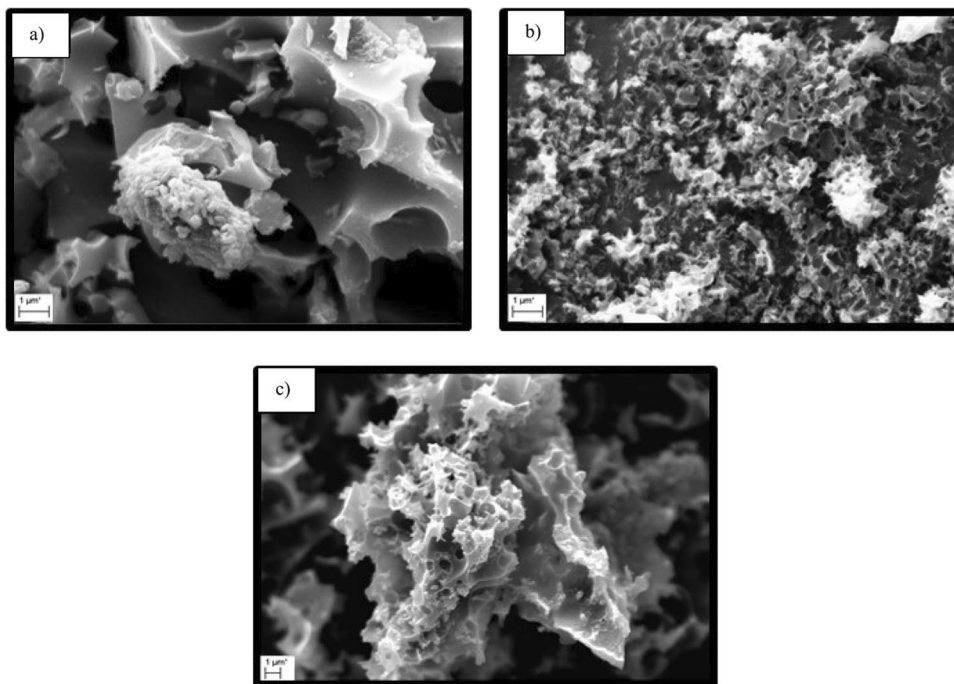
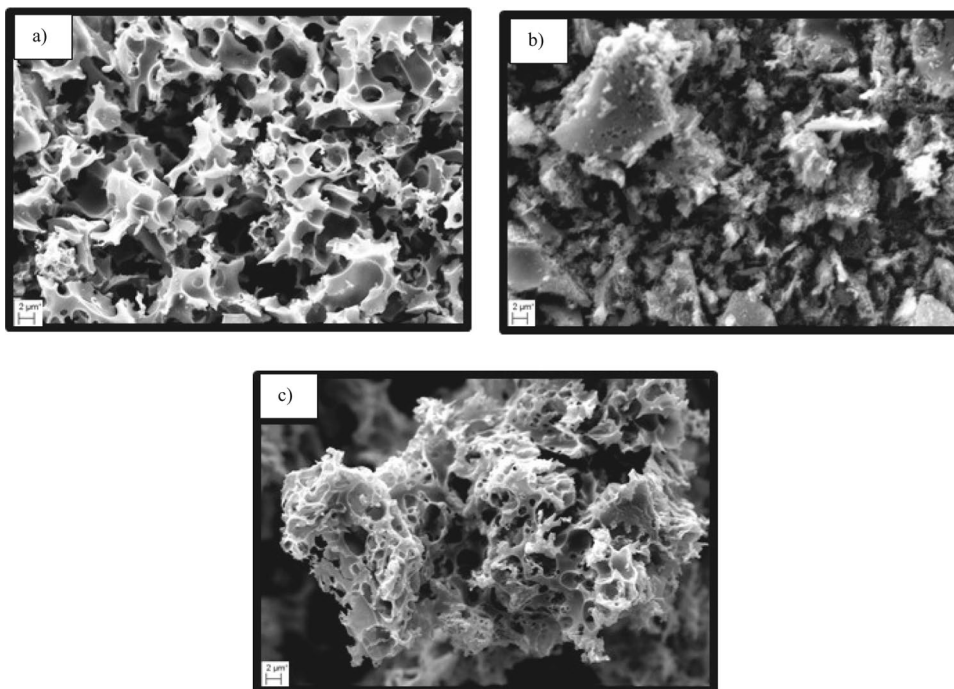


Fig. 6 SEM images for activated BP hydrochar (Mag: 5k X): **a** BP-180, **b** BP-200, and **c** BP-220

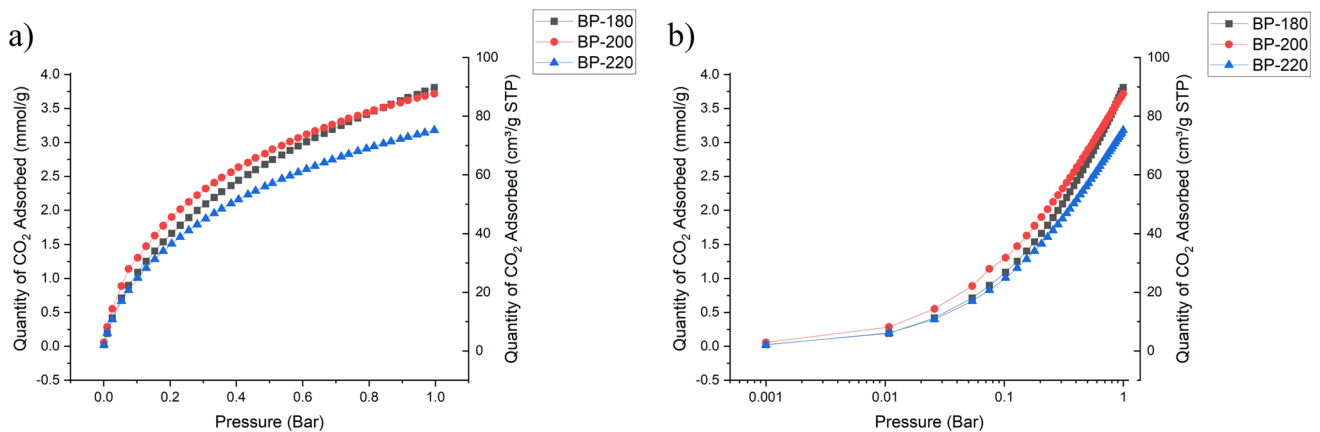


The adsorption of CO_2 on the surface is mainly due to the physisorption mechanism. It is seen that, even with the variation in temperature, adsorption does not necessarily need any activation energy. CO_2 does not have a dipole but a strong quadrupole moment. Due to its linear shape and polar bonds on either end, CO_2 can easily interact with active sites on the char surface (Goel et al. 2021). The addition of

nitrogenous functional groups can increase the physisorption of CO_2 on char surfaces because of the strong interaction between the acidic CO_2 and basic nitrogenous surface functional groups (Creamer and Gao, 2016). Huang et al. studied the CO_2 adsorption performance on hydrochar obtained from garlic peel (Huang et al. 2019). That study clearly indicated a decrease in the CO_2 adsorption with the increase in

Table 2 Pore structure parameters calculated from S_{BET} analysis and CO_2 uptakes at 1 bar for KOH-activated BP hydrochar samples and comparison with other work

Sample	HTC temperature (°C)	S_{BET} (m^2/g)	V_t (cm^3/g)	CO_2 uptake at 25 °C (mmol/g)	References
BP-180	180	243.4	0.0931	3.8	
BP-200	200	154.6	0.0798	3.71	
BP-220	220	71.72	0.0223	3.18	
Feedstock	–	1.1	–	–	Yusuf et al. 2020
HCT-200	200	1.601	–	–	Yusuf et al. 2020
HCT-300	300	9.194	–	–	Yusuf et al. 2020
Africa palm		1250	0.61	4.4	(Ello et al. 2013)
Argan shell		1889	0.87	5.63	(Boujibar et al. 2018)
Camphor leaves		1146	0.546	3.74	(Xu et al. 2018)
Carrot peels		1379	0.58	4.18	(Serafin et al. 2017)
Chicken manure waste		22.22	0.047	1.95	(Yildiz et al. 2019)
Coconut shell		1535	0.6	4.8	(Chen et al. 2016)
		1383	0.56	4	(Yue et al. 2018)
Empty fruit brunch		2510	1.05	3.712	(Parshetti et al. 2015)
Enteromorpha		60.2	0.16	0.52	(Ding and Liu, 2020)
Fern leaves		1593	0.74	4.12	(Serafin et al. 2017)
Garlic peel		947	0.51	4.22	(Huang et al. 2019)
Grass cuttings		1118	0.47	3.97	(Pang et al. 2021)
Hazelnut shell		1696	0.7	4.23	(Pang et al. 2021)
		1354	0.59	4.16	(Pang et al. 2021)
Jujun grass		1512	0.74	4.9	(Coromina et al. 2016)
Pine cone shell		3135	0.71	4.73	(Li et al. 2016)
Pine nutshells		1486	0.64	5	(Deng et al. 2014)
Pomegranate		585	0.28	4.11	(Serafin et al. 2017)
Rice husk		1041	0.53	4.16	(Li et al. 2015)
		1162	0.685	1.8	(Liu et al. 2019b)
Sargassum		291.8	0.24	1.05	(Ding and Liu, 2020)
Sugarcane bagasse		1113	0.574	4.8	(Han et al. 2019)
Vine shoots		1671	0.67	5.4	(Manyà et al. 2018)
Water chest nutshell		1517	1.08	2.95	(Li et al. 2020)

**Fig. 7** a Linear plot and b Semilogarithmic plot of CO_2 uptake isotherm of BP hydrochar samples

temperature suggesting physisorption mechanism. The findings are also supported by Zubbri et al. who examined CO₂ capture on KOH-activated hydrochar obtained from rambutan peel (Zubbri et al. 2021). Very weak values of activation energy were determined using the Avrami kinetic model, demonstrating that the mechanism is mainly of the physisorption type. The increase in the CO₂ adsorption is heavily dependent on large surface area and high micropore volume of hydrochar samples (Li et al. 2020). The data of Table 2 were further subjected to analysis of variance (ANOVA) to determine the statistical significance of S_{BET} and V_t on CO₂ uptake at 25 °C. The statistical model had a coefficient of determination of 0.91. The highest contribution was obtained from S_{BET} (71%) with a p -value of 0.0001 at 95% level of confidence. The result indicated that the surface area has a very high influence on the CO₂ adsorption capacity of the char. This is confirmed by the results obtained with BP hydrochar since BP-180, with the highest CO₂ uptake, possesses the maximum surface area and pore volume.

Meanwhile, uptakes, surface areas and pore volumes for BP-200 and BP-220 are much lower. This indicates that CO₂ uptake depends on microporosity. It can be observed from Fig. 7a that the CO₂ uptake at 1 bar decreases with an increase in the process temperature. Previous studies have indicated that CO₂ uptake first increases and then decreases with process temperature, suggesting that an appropriate temperature is needed to create the desired pore for CO₂ capture under a specific condition. It can be determined from this study that, for optimal CO₂ adsorption at 1 bar on the BP hydrochar, the process temperature should be lower than 200 °C. For adsorption at lower pressure < 0.8 bar, BP-200 seems to perform better than BP-180 for CO₂ uptake. This might be because, at low pressure, adsorption takes place via narrow micropores in monolayer, and BP-200 has a better narrow pore structure which helps in adsorption at low pressure. At a higher pressure, adsorption occurs via a multilayer, sometimes in mesopore, which might be better developed in BP-180 (Li et al. 2015; Shi et al. 2019). It is revealed that CO₂ uptake performance can be potentially enhanced by the adsorbent's microporous characteristics and not micropore volume. The low correlation between total pore volume and surface area was also observed by (Ma et al. 2020). The electrostatic interaction on the surface with CO₂ increases due to the presence of oxygen functional groups. We believe that the same phenomena lead to higher CO₂ uptake in BP-180 with a relatively low surface area compared to other hydrochars in the literature. The presence of high oxygen is also confirmed by the elemental composition in Table 1 and by peaks obtained in the FTIR analysis.

It should be noted that CO₂ uptake on N-doped hydrochar derived from longan shells and water chestnut biomass is higher because of the introduction of nitrogen atoms (Huang et al. 2019). But the BP-180 was obtained due to

the low-cost HTC process along with KOH activation and without nitrogen doping. This makes KOH-activated BP waste hydrochar a suitable low-cost adsorbent for CO₂ under ambient conditions.

Conclusions

Banana peel was converted to hydrochar products via HTC at temperatures between 180 °C and 220 °C. The HTC samples were activated with KOH at 700 °C under nitrogen flow. The experimental results showed good porosity and high surface area of the activated hydrochar. KOH activation promoted an increase in porosity. The results showed that the HTC process temperature plays a significant role in yield and other physicochemical properties. Carbon yield is directly related to process temperature. Compared to other studies on BP derived hydrochar at the same temperature of 200 °C, the carbon content in the hydrochar has increased due to an increase in residence time. Carbon and oxygen were mainly found by SEM–EDX analysis. This was confirmed by FTIR analysis, where the presence of the C=O and C–O bonds along with C≡C and C=C bonds was observed. The highest CO₂ uptake of 3.8 mmol/g was noted for BP-180 at 1 bar and a temperature of 25 °C due to high microporosity and a surface area of 243.4 m²/g.

Funding Open access funding provided by Manipal Academy of Higher Education, Manipal.

Data availability Data will be made available on request.

Declarations

Competing interests There are no competing or conflicts of interest to declare.

Open Access This article is licensed under a Creative Commons Attribution 4.0 International License, which permits use, sharing, adaptation, distribution and reproduction in any medium or format, as long as you give appropriate credit to the original author(s) and the source, provide a link to the Creative Commons licence, and indicate if changes were made. The images or other third party material in this article are included in the article's Creative Commons licence, unless indicated otherwise in a credit line to the material. If material is not included in the article's Creative Commons licence and your intended use is not permitted by statutory regulation or exceeds the permitted use, you will need to obtain permission directly from the copyright holder. To view a copy of this licence, visit <http://creativecommons.org/licenses/by/4.0/>.

References

- Boujibar O, Souikny A, Ghamouss F, Achak O, Dahbi M, Chafik T (2018) CO₂ capture using N-containing nanoporous activated

- carbon obtained from argan fruit shells. *J Environ Chem Eng* 6:1995–2002. <https://doi.org/10.1016/j.jece.2018.03.005>
- Brosse N, Dufour A, Meng X, Sun Q, Ragauskas A (2012) Miscanthus: a fast-growing crop for biofuels and chemicals production. *Biofuels Bioprod Biorefining* 6:580–598. <https://doi.org/10.1002/bbb.1353>
- Bui M, Adjiman CS, Bardow A, Anthony EJ et al (2018) Carbon capture and storage (CCS): the way forward. *Energy Environ Sci* 11(5):1062–1176. <https://doi.org/10.1039/c7ee02342a>
- Chen J, Yang J, Hu G, Hu X, Li Z, Shen S (2016) Enhanced CO₂ capture capacity of nitrogen-doped biomass-derived porous carbons. *ACS Sustain Chem Eng* 4(3):1439–1445. <https://doi.org/10.1021/acssuschemeng.5b01425>
- Choi A, Drese JH, Jones CW (2009) Adsorbent materials for carbon dioxide capture from large anthropogenic point sources. *Chem Sus Chem* 2(9):796–854. <https://doi.org/10.1002/cssc.200900036>
- Chue KT, Kim JN, Yoo YJ, Cho SH, Yang RT (1995) Comparison of activated carbon and zeolite 13X for CO₂ recovery from flue gas by pressure swing adsorption. *Indus Eng Chem Res* 34(2):591–598. <https://doi.org/10.1021/ie00041a020>
- Coromina HM, Walsh DA, Mokaya R (2016) Biomass-derived activated carbon with simultaneously enhanced CO₂ uptake for both pre and post combustion capture applications. *J Mater Chem A* 4(1):280–289. <https://doi.org/10.1039/C5TA09202G>
- Cuéllar-Franca RM, Azapagic A (2015) Carbon capture, storage and utilisation technologies: A critical analysis and comparison of their life cycle environmental impacts. *J CO₂ Utilization* 9:82–102. <https://doi.org/10.1016/j.jcou.2014.12.001>
- Dadrasnia A, Usman MM, Omar R, Ismail S, Abdullah R (2020) Potential use of *Bacillus* genus to control of bananas diseases: approaches toward high yield production and sustainable management. *J King Saud Univ Sci* 32:2336–2342. <https://doi.org/10.1016/j.jksus.2020.03.011>
- Deepak KR, Mohan S, Dinesha P, Balasubramanian R (2023) CO₂ uptake by activated hydrochar derived from orange peel (*Citrus reticulata*): Influence of carbonization temperature. *J Environ Manag* 342:118350. <https://doi.org/10.1016/j.jenvman.2023.118350>
- Deng S, Wei H, Chen T, Wang B, Huang J, Yu G (2014) Superior CO₂ adsorption on pine nut shell-derived activated carbons and the effective micropores at different temperatures. *Chem Eng J* 253:46–54. <https://doi.org/10.1016/j.cej.2014.04.115>
- Ding S, Liu Y (2020) Adsorption of CO₂ from flue gas by novel seaweed-based KOH-activated porous biochars. *Fuel* 260:116382. <https://doi.org/10.1016/j.fuel.2019.116382>
- Dong X, Guo S, Wang H, Wang Z, Gao X (2019) Physicochemical characteristics and FTIR-derived structural parameters of hydrochar produced by hydrothermal carbonisation of pea pod (*Pisum sativum* Linn.) waste. *Biomass Convers Biorefinery* 9:531–540. <https://doi.org/10.1007/s13399-018-0363-1>
- Ello AS, de Souza LC, Trokourey A, Jaroniec M (2013) Development of microporous carbons for CO₂ capture by KOH activation of African palm shells. *J CO₂ Utilization* 235:38. <https://doi.org/10.1016/j.jcou.2013.07.003>
- Global monitoring laboratory (2022) Trends in atmospheric carbon dioxide [WWW Document]. US Dep. Commer. URL <https://gml.noaa.gov/ccgg/trends/weekly.html> (accessed 11.26.22)
- Goel C, Mohan S, Dinesha P (2021) CO₂ capture by adsorption on biomass-derived activated char: a review. *Sci Total Environ* 798:149296. <https://doi.org/10.1016/j.scitotenv.2021.149296>
- Han J, Zhang L, Zhao B, Qin L, Wang Y, Xing F (2019) The N-doped activated carbon derived from sugarcane bagasse for CO₂ adsorption. *Indus Crops Prod* 128:290–297. <https://doi.org/10.1016/j.indcrop.2018.11.028>
- Hong WY (2022) A techno-economic review on carbon capture, utilisation and storage systems for achieving a net-zero CO₂ emissions future. *Carbon Capture Sci Technol* 3:100044. <https://doi.org/10.1016/j.ccost.2022.100044>
- Huang G, Liu Y, Wu X, Cai J (2019) Activated carbons prepared by the KOH activation of a hydrochar from garlic peel and their CO₂ adsorption performance. *New Carbon Mater* 34:247–257. [https://doi.org/10.1016/S1872-5805\(19\)60014-4](https://doi.org/10.1016/S1872-5805(19)60014-4)
- Hussein HS, Shaarawy HH, Hussien NH, Hawash SI (2019) Preparation of nano-fertilizer blend from banana peels. *Bull Natl Res Cent* 43:26. <https://doi.org/10.1186/s42269-019-0058-1>
- Mordor intelligence (2022) Banana market—growth, trends, Covid-19 impact, and forecasts (2022–2027) [WWW Document]. Mordor Intell. URL <https://www.mordorintelligence.com/industry-reports/banana-market> (accessed 12. 6. 22)
- Kabenge I, Omulo G, Banadda N, Seay J, Zziwa A, Kiggundu N (2018) Characterization of banana peels wastes as potential slow pyrolysis feedstock. *J Sustain Dev* 11:14–24. <https://doi.org/10.5539/jsd.v11n2p14>
- Kambo HS, Dutta A (2015) A comparative review of biochar and hydrochar in terms of production, physico-chemical properties and applications. *Renew Sustain Energy Rev* 45:359–378. <https://doi.org/10.1016/j.rser.2015.01.050>
- Khan N, Mohan S, Dinesha P (2021) Regimes of hydrochar yield from hydrothermal degradation of various lignocellulosic biomass: a review. *J Clean Prod* 288:125629. <https://doi.org/10.1016/j.jclepro.2020.125629>
- Lee E-H, Yeom H-J, Ha M-S, Bae D-H (2010) Development of banana peel jelly and its antioxidant and textural properties. *Food Sci Biotechnol* 19:449–455. <https://doi.org/10.1007/s10068-010-0063-5>
- Li D, Ma T, Zhang R, Tian Y, Qiao Y (2015) Preparation of porous carbons with high low-pressure CO₂ uptake by KOH activation of rice husk char. *Fuel* 139:68–70. <https://doi.org/10.1016/j.fuel.2014.08.027>
- Liu X, Sun C, Liu H, Tan WH, Wang W, Snape C (2019) Developing hierarchically ultra-micro/mesoporous biocarbons for highly selective carbon dioxide adsorption. *Chem Eng J* 361:199–208. <https://doi.org/10.1016/j.cej.2018.11.062>
- Li Q, Liu S, Peng W, Zhu W, Wang L, Chen F, Shao J, Hu X (2020) Preparation of biomass-derived porous carbons by a facile method and application to CO₂ adsorption. *J Taiwan Inst Chem Eng* 116:128–136. <https://doi.org/10.1016/j.jtice.2020.11.001>
- Li K, Tian S, Jiang J, Wang J, Chen X, Yan F (2016) Pine cone shell-based activated carbon used for CO₂ adsorption. *J Mat Chem A* 4(14):5223–5234. <https://doi.org/10.1039/C5TA09908K>
- Liew RK, Nam WL, Chong MY, Phang XY, Su MH, Yek PNY, Ma NL, Cheng CK, Chong CT, Lam SS (2018) Oil palm waste: an abundant and promising feedstock for microwave pyrolysis conversion into good quality biochar with potential multi-applications. *Process Saf Environ Prot* 115:57–69. <https://doi.org/10.1016/j.psep.2017.10.005>
- Liu C, Wang H, Karim AM, Sun J, Wang Y (2014) Catalytic fast pyrolysis of lignocellulosic biomass. *Chem Soc Rev* 43:7594–7623. <https://doi.org/10.1039/c3cs60414d>
- Liu F, Yu R, Guo M (2017) Hydrothermal carbonization of forestry residues: influence of reaction temperature on holocellulose-derived hydrochar properties. *J Mater Sci* 52:1736–1746. <https://doi.org/10.1007/s10853-016-0465-8>
- Leung D, Caramanna G, Maroto-Valer MM (2014) An overview of current status of carbon dioxide capture and storage technologies. *Renew Sustain Energy Rev* 39:426–443. <https://doi.org/10.1016/j.rser.2014.07.093>
- Ma X, Yang Y, Wu Q, Liu B, Li D, Chen R (2020) Underlying mechanism of CO₂ uptake onto biomass-based porous carbons: do

- adsorbents capture CO₂ chiefly through narrow micropores? Fuel 282:118727. <https://doi.org/10.1016/j.fuel.2020.118727>
- Manyà JJ, González B, Azuara M, Arner G (2018) Ultra-microporous adsorbents prepared from vine shoots-derived biochar with high CO₂ uptake and CO₂/N₂ selectivity. Chem Eng J 345:631–639. <https://doi.org/10.1016/j.cej.2018.01.092>
- Nieto N, Noya O, Iturrondobeitia A, Sanchez-Fontecoba P, Pérez-López U, Palomares V, Lopez-Urionabarrenechea A, Rojo T (2022) On the road to sustainable energy storage technologies: synthesis of anodes for Na-Ion batteries from biowaste. Batteries 8:28. <https://doi.org/10.3390/batteries8040028>
- Olivier JGJ, Peters JAHW (2020) Trends in global CO₂ and total greenhouse gas emissions [WWW Document]. URL https://www.pbl.nl/sites/default/files/downloads/pbl-2020-trends-in-global-co2-and-total-greenhouse-gas-emissions-2020-report_4331.pdf (accessed 12.6.22)
- Pang R, Lu T, Shao J, Wang L, Wu X, Qian X, Hu X (2021) Highly efficient nitrogen-doped porous carbonaceous CO₂ adsorbents derived from biomass. Energy Fuels 35(2):1620–1628. <https://doi.org/10.1021/acs.energyfuels.0c03832>
- Parshetti GK, Chowdhury S, Balasubramanian R (2015) Biomass derived low-cost microporous adsorbents for efficient CO₂ capture. Fuel 148:246–254. <https://doi.org/10.1016/j.fuel.2015.01.032>
- Perlack R (2003) Feedstock cost analysis of corn stover residues for further processing. Energy 28:1395–1403. [https://doi.org/10.1016/s0360-5442\(03\)00123-3](https://doi.org/10.1016/s0360-5442(03)00123-3)
- Pokharel P, Kwak J-H, Ok YS, Chang SX (2018) Pine sawdust biochar reduces GHG emission by decreasing microbial and enzyme activities in forest and grassland soils in a laboratory experiment. Sci Total Environ 625:1247–1256. <https://doi.org/10.1016/j.scitotenv.2017.12.343>
- Selvan RK, Lee YS (2016) Pt decorated Artocarpus heterophyllus seed derived carbon as an anode catalyst for DMFC application. RSC Adv 6(67):62680–94. <https://doi.org/10.1039/C6RA05833G>
- Sekoai PT, Yoro KO (2016) Biofuel development initiatives in Sub-Saharan Africa: opportunities and challenges. Climate. <https://doi.org/10.3390/cli4020033>
- Sharma HB, Dubey BK (2020) Co-hydrothermal carbonization of food waste with yard waste for solid biofuel production: hydrochar characterization and its pelletization. Waste Manag 118:521–533. <https://doi.org/10.1016/j.wasman.2020.09.009>
- Shi W, Wang R, Liu H, Chang B, Yang B, Zhang Z (2019) Biowaste-derived 3D honeycomb-like N and S dual-doped hierarchically porous carbons for high-efficient CO₂ capture. RSC Adv 9:23241–23253. <https://doi.org/10.1039/C9RA03659H>
- Singh J, Bhunia H, Basu S (2019) Adsorption of CO₂ on KOH activated carbon adsorbents: effect of different mass ratios. J Environ Manag 250:109457. <https://doi.org/10.1016/j.jenvman.2019.109457>
- Serafin J, Narkiewicz U, Morawski AW, Wróbel RJ, Michalkiewicz B (2017) Highly microporous activated carbons from biomass for CO₂ capture and effective micropores at different conditions Journal of CO₂ Utilization. 18:73–79. <https://doi.org/10.1016/j.jcou.2017.01.006>
- van Soest HL, de Boer HS, Roelfsema M, den Elzen MGJ, Admiraal A, van Vuuren DP, Hof AF, van den Berg M, Harmsen MJHM, Gernaat DEHJ, Forsell N (2017) Early action on Paris agreement allows for more time to change energy systems. Clim Change 144:165–179. <https://doi.org/10.1007/s10584-017-2027-8>
- Wang Q, Luo J, Zhong Z, Borgna A (2011) CO₂ capture by solid adsorbents and their applications: current status and new trends. Energy Environ Sci 4(1):42–55. <https://doi.org/10.1039/c0ee00064g>
- Xu J, Shi J, Cui H, Yan N, Liu Y (2018) Preparation of nitrogen doped carbon from tree leaves as efficient CO₂ adsorbent. Chem Phys Lett 711:107–112. <https://doi.org/10.1016/j.cplett.2018.09.038>
- Xu Z, Ma X, Liao J, Osman SM, Wu S, Luque R (2022) Effects on the physicochemical properties of hydrochar originating from deep eutectic solvent (urea and ZnCl₂)-assisted hydrothermal carbonization of Sewage Sludge. ACS Sustain Chem Eng 10:4258–4268. <https://doi.org/10.1021/acssuschemeng.2c00086>
- Yabalak E, Elneccar F (2022) Evaluation of watermelon peel, banana peel and bay leaves hydrochars as green catalysts in the degradation of malachite green by thermally activated persulfate oxidation method. J Environ Manag 304:114311. <https://doi.org/10.1016/j.jenvman.2021.114311>
- Yildiz Z, Kaya N, Topcu Y, Uzun H (2016) Pyrolysis and optimization of chicken manure wastes in fluidized bed reactor: CO₂ capture in activated bio-chars. Process Saf Environ Prot 130:297–305. <https://doi.org/10.1016/j.psep.2019.08.011>
- Yue L, Xia Q, Wang L, Wang L, DaCosta H, Yang J, Hu X (2018) CO₂ adsorption at nitrogen-doped carbons prepared by K₂CO₃ activation of urea-modified coconut shell. J Colloid Interface Sci 511:259–267. <https://doi.org/10.1016/j.jcis.2017.09.040>
- Yusuf I, Flagiello F, Ward NI, Arellano H, Avignone-rossa C, Felipe-sotelo M (2020) Valorisation of banana peels by hydrothermal carbonisation: potential use of the hydrochar and liquid by-product for water purification and energy conversion. Bioresour Technol Rep. <https://doi.org/10.1016/j.biteb.2020.100582>
- Zhao Z, Ma C, Chen F, Xu G, Pang R, Qian X, Shao J, Hu X (2021) Water caltrop shell-derived nitrogen-doped porous carbons with high CO₂ adsorption capacity. Biomass Bioenerg 145:105969. <https://doi.org/10.1016/j.biombioe.2021.105969>
- Zubbri NA, Mohamed AR, Lahijani P, Mohammadi M (2021) Low temperature CO₂ capture on biomass-derived KOH-activated hydrochar established through hydrothermal carbonization with water-soaking pre-treatment. J Environ Chem Eng 9:105074. <https://doi.org/10.1016/j.jece.2021.105074>

Publisher's Note Springer Nature remains neutral with regard to jurisdictional claims in published maps and institutional affiliations.